Monolayer-Protected Anionic Au Nanoparticles Walk into Lipid Membranes Step-by-Step

Federica Simonelli[1], *Davide Bochicchio*[1], *Riccardo Ferrando*[2] *and Giulia Rossi*[1]*

[1] Physics Department, University of Genoa, Via Dodecaneso 33, 16146 Genoa, Italy

[2] Chemistry Department, University of Genoa, Via Dodecaneso 31, 16146 Genoa, Italy

AUTHOR INFORMATION

Corresponding Author

*rossig@fisica.unige.it

The design of ligand-protected metal nanoparticles (NPs) with biomedical applications relies on the understanding, at molecular level, of their interactions with cell membranes. Here we study, via unbiased coarse grained molecular dynamics simulations, the kinetics and the thermodynamics of the interaction between anionic ligand-protected gold NPs and model lipid membranes. The NP-membrane interaction is a three-step process: electrostatics-driven adhesion to the membrane surface, hydrophobic contact and final embedding in the membrane core via anchoring of the charged ligands to both membrane leaflets. Our free energy calculations show that anchoring is highly favorable and not reversible. Furthermore, we show that the interaction pathway of NPs with random surface arrangement of anionic and hydrophobic ligands is

characterized by two metastable configurations: adsorbed at the membrane surface, and membrane-embedded. Patched ligand arrangements, instead, lead to the stabilization of a third, intermediate metastable configuration, resulting in a much slower kinetics of interaction with the membrane.

TOC GRAPHICS

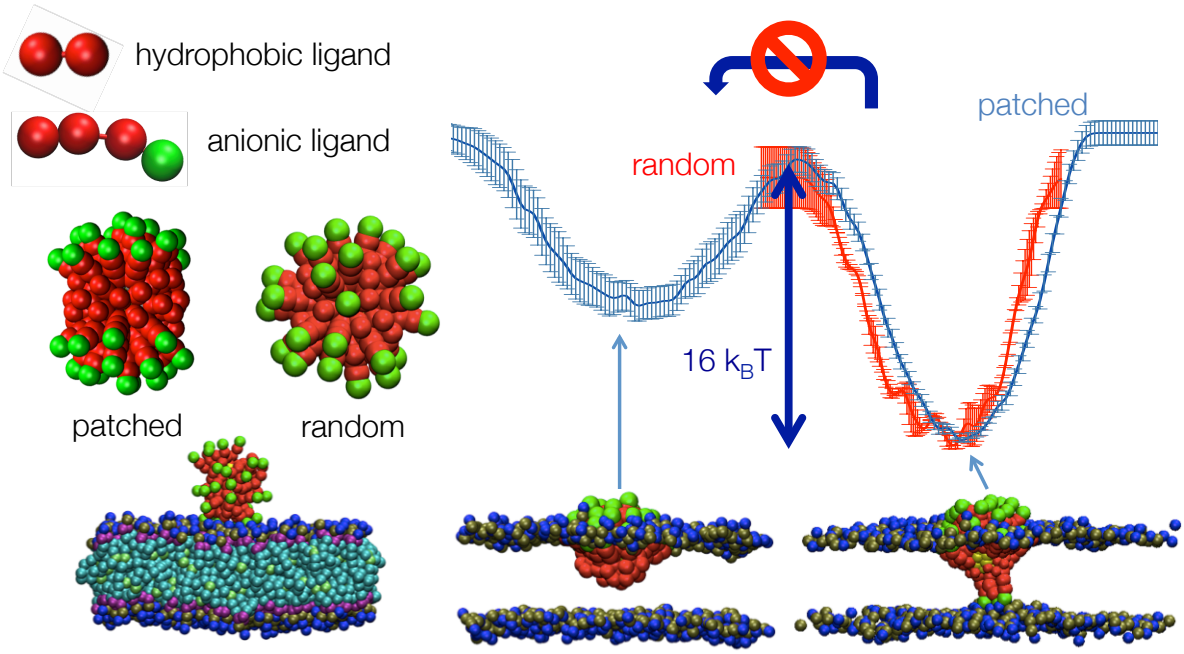

6

KEYWORDS Coarse graining, molecular dynamics, free energy calculations

Monolayer-protected metal nanoparticles (NP) play more and more important roles as diagnostic and therapeutic agents[1–4]. Cell membranes are the first barriers encountered by NPs

entering our organism, and the understanding of the molecular processes that drive the NP-membrane interaction is crucial to the design of NPs with biomedical applications. The membrane-NP interaction results from a complex interplay of electrostatics, hydrophobic interactions, ligand composition, surface ligand arrangement and, on the membrane side, lipid composition and phase.

The interest in monolayer-protected gold NPs is motivated by the relatively inert and thus biocompatible nature of Au, and by its electronic and optical properties[1–3]. Gold is also easily passivated via Au-S bonds[5] to organothiolates, whose terminal groups can be chemically designed to finely tune the NP degree of hydrophobicity.

Many open questions are still unanswered. What is the role played by electrostatics at determining the type of interaction with lipid membranes? Cationic NPs are generally reported to be more toxic than anionic NPs[6–8]. Recent neutron scattering data by Tatur *et al*. [8], suggest that anionic Au NPs may not enter the hydrophobic core of zwitterionic lipid membranes at all, simply adhering to their surface in the fluid phase and leading to lipid dehydration. Van Lehn *et al*.[9], indicate a stable binding to zwitterionic bilayers and the possibility of passive membrane translocation. Recent centrifugation-based assays suggest that PEG-passivated Ag NPs, bearing a small negative charge, do interact with zwitterionic vesiscles affecting their precipitation behavior[10]. Finer details concerning the arrangement of the charged ligands on the NP surface might affect the NP-membrane interaction and possibly explain the broad range of behaviors that so far have been observed experimentally[11–13].

In the last couple of years, computational modeling has contributed to sketch a possible mechanism of interaction of anionic NP with zwitterionic lipid membranes. The first phases of such interaction have been elucidated via both atomistic[14–16] and coarse-grained[17] molecular

dynamics simulations. It is now clear that electrostatic attraction between the charged ligands and the polar heads of zwitterionic lipid in the fluid phase drives the adhesion of the NP to the membrane surface. At the other end of the pathway, thermodynamics-based, implicit solvent and implicit bilayer models indicate that the most stable NP transmembrane state may correspond to the so-called "snorkeling" configuration[9]. In this configuration the centre of mass of the NP is embedded in the membrane core, while the charged ligand terminals stably interact with the lipid head regions of both leaflets. The all-atom (AA) molecular dynamics (MD) simulations performed by Heikkilä *et al*[14]. and the coarse grained ones performed by Gkeka *et al*[17]. could not observe any spontaneous penetration of the NP into the membrane core, due to the limited sampling time. Van Lehn *et al*. observed via AA simulations the spontaneous insertion of the NPs only at the highly curved edge of a lipid bicelle[15], where the process is mediated by the protrusion of a lipid tail out of the hydrophobic membrane core. When interacting with a flat membrane, the insertion process has been reproduced only via biased simulations, either favouring a lipid-ligand hydrophobic contact by imposing an external driving potential on one lipid tail[16], or directly forcing the NP in the centre of the bilayer by removal of the overlapping lipids[17]. So far, no unbiased simulation of the insertion process has been performed and the kinetics of the process has not been described.

Concerning the influence of the NP surface pattern, no clear picture has emerged so far from either thermodynamics-based models or MD simulations. The implicit bilayer and implicit solvent model by Van Lehn *et al*. does not predict any substantial difference in the water-membrane free energy of transfer of NPs with random or striped ligand patterns[9,18]. Gkeka *et al*., based on a rigid-sphere model of the NP, calculated the water-membrane free energy of transfer of NPs with homogeneous or random arrangement of hydrophobic and charged beads on the

surface, and concluded that the NPs with a homogeneous pattern should passively translocate through the membrane more easily than those with a random arrangement[19].

In this paper, we present coarse-grained unbiased MD simulation of the whole interaction process, and conclude that anionic gold NPs do insert in the membrane core, the final snorkeling configuration being energetically highly favorable. Our unbiased simulations show that the insertion process is indeed mediated by the spontaneous protrusion of a lipid tail that initiates the NP-membrane hydrophobic contact. This stage is followed by the dropping of a charged ligand (an "anchor") to the opposite leaflet, thus stabilizing the NP-membrane complex. Eventually, more and more anchors are dropped leading to the final snorkeling configuration. Our free-energy calculations show that the anchoring process is almost irreversible.

We furthermore show that the kinetics of the process depends on the NPs' ligand composition and surface arrangement. Our calculations show that the interaction free energy profile of the NPs with a random surface arrangement of anionic and hydrophobic ligands is characterized by two metastable minima, corresponding to the surface-adsorbed configuration and to the snorkeling configuration. NPs whose ligands form large hydrophobic or anionic surface patches, instead, go through three metastable configurations. The transition from the adsorbed state to the snorkeling state is indeed slowed down by a significant energy barrier which stabilizes an intermediate metastable state, in which the NP is semi-adsorbed.

Coarse grained model. We considered a $Au_{144}(SR)_{60}$ NP, R being either a hydrophobic octanethiol ligand (OT) or an anionic 11-mercaptoundecane sulphonate (MUS). The diameter of the Au core is about 2 nm (Supplementary Figure S1), while the monolayer-protected NP has an overall diameter of about 4 nm. We modeled the Au-Au and Au-S interactions using an elastic network, while we developed a coarse-grained (CG) model of the ligands based on the popular

Martini force field[20] (Fig. 1). At CG level the OT ligands are modeled as a chain of 2 hydrophobic (type C_1) beads. The MUS ligands are described by 3 hydrophobic beads (Martini type C_1) and one negatively charged terminal bead (type Q_{da}). The details of the parameterization can be found in the Supporting Information. We remark here that our coarse grained description does not distinguish between, e.g., mercaptoundecanoic acid and mercaptoundecane sulphonate, allowing for the direct comparison with several independent previous computational (AA) and experimental works.

One possible reason of concern about the use of CG models to study anionic NP-membrane interactions is the treatment of electrostatic interactions. Contrary to AA models, which parameterization includes long-range electrostatics, the Martini force field sharply cuts off Coulomb interactions at short distances (1.2 nm). In order to validate our CG model in this respect, we compared the three-dimensional spatial distributions of the passivated Au NPs in water to previous atomistic simulations (Supplementary Figure S2 and S3). We obtained a satisfactory overlapping of all the partial radial distribution functions (RDF) for hydrophobic moieties, charged ligands, counterions and water. In previous simulations of the interaction between charged dendrimers and lipid membranes, Lee and Larson[21] proposed to include the long-range electrostatic contributions into the MARTINI force field by implementing the Particle-Mesh-Ewald method. We tested this approach as well, but observed no substantial changes of the RDFs (Supplementary Figure S4), together with obvious computational disadvantages. We calculated the Debye length, which measures the screening effects of counterions in an electrolytic solution, for the Na+ counterions surrounding our anionic NP in water. The Debye length can be deduced from the fitting of the counterions RDF at long distances to the Debye-Hückel distribution $f(r) = Ae^{-Br} + C$, where A, B, C are positive

parameters and *r* is the distance from the centre of the charged NP. The Debye length L_D is the inverse of B. From the fitting procedure, applied to the ion RDFs as obtained with plain Coulomb cut-off, the Debye length is 0.18 nm (Supplementary Figure S5), in good agreement with the value obtained by Heikkilä *et al*.[22] via AA simulations (L_D = 0.20 nm). More details on the model validation can be found in the Supporting Information.

We looked at three different NPs: a) MUS:OT 2:1 ligand composition, with random surface arrangement of the ligands b) MUS:OT 1:1, random and c) MUS:OT, 1:1 with a patched arrangement, made of a central hydrophobic (OT) stripe flanked by two charged (MUS) poles. All NPs are shown in Fig.1, and the protocol for their construction is described in the Supporting Information. Our model lipid membrane is a patch of 512 phosphatidylcholine (POPC) lipids.

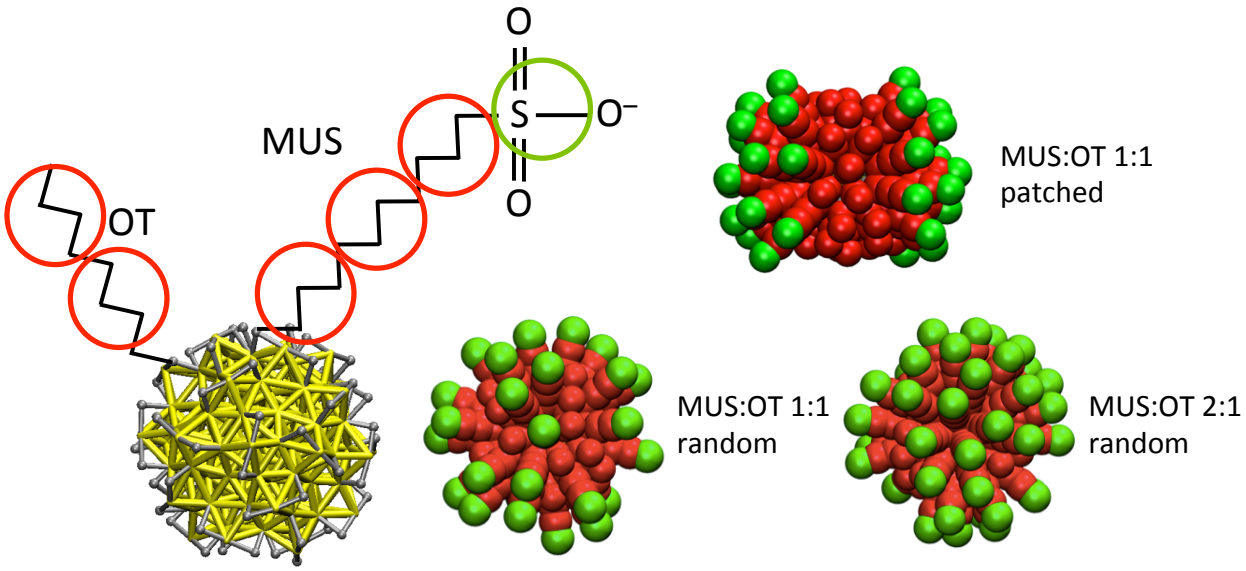

Figure 1. Left: the Au-S elastic network (Au in yellow, S in grey). The atomistic structure of the two ligands is shown in black, while the CG model used in this work is shown by the red hydrophobic beads and by the green, negatively charged beads. Right: the three NPs used in the simulations.

The NP-membrane interaction is a 3-stage process. For all the NP compositions and ligand arrangements we considered, the NP-membrane interaction is a three-stage process, as shown in Figure 2. First, the NP adsorbs at the membrane surface (stage 1). Second, a hydrophobic contact is established between the hydrophobic moieties of the ligands and the lipid tails (stage 2). Third, one or more charged ligand terminals cross the hydrophobic core of the lipid membrane to bind to the head region of the opposite leaflet (stage 3).

Stage 1: NP adsorption at the membrane surface. The first interaction stage is the adhesion of the charged NP to the head region of the membrane. In our 10 or 20 μs runs the time that the NPs spent at the membrane surface (before the hydrophobic contact with the membrane core was established) was of the order of several μs. The arrangement of the ligands on the NP surface affects the strength of the interaction with the lipid heads. As shown in Supplementary Figure S6, the random MUS:OT 1:1 NPs are the least stably bound, with frequent detachments from the membrane. The random MUS:OT 2:1 are more stably bound, even if short detachments can be observed. The patched MUS:OT 1:1 NPs never detaches from the membrane surface within the simulated time range.

Stage 2: a hydrophobic contact is established. The second interaction stage consists in the formation of a hydrophobic contact between the membrane core and the hydrophobic moieties of the ligands, leading to a partial embedding of the NP into the membrane. Our unbiased simulations show that the hydrophobic contact is initiated by the protrusion of one lipid tail to the head region (Figure 2b and 2c). This process, which we here observe in all our unbiased MD runs, is consistent with what reported, for the case of highly curved membranes, by Van Lehn *et al*.[15] Once the lipid protrusion has triggered the formation of the hydrophobic contact, the NP's

ligands rearrange in such a way as to expose their hydrophobic moieties to the membrane tail region (Figure 2d). While the centre of mass of the NP gets embedded in the head region, most of the negatively charged terminals of the ligands create favorable electrostatic contact with the choline groups of the lipids. We monitored the number of hydrophobic-hydrophobic and charge-charge contacts between the NP and the ligands (Supplementary Figure S7), and both types of contacts increase when the hydrophobic contact is established, suggesting that the process is enthalpically favored. While in stage 2, the patched NPs maintain a fixed orientation, with the plane of the central hydrophobic stripe aligned to the membrane normal (see Supplementary Figure S8).

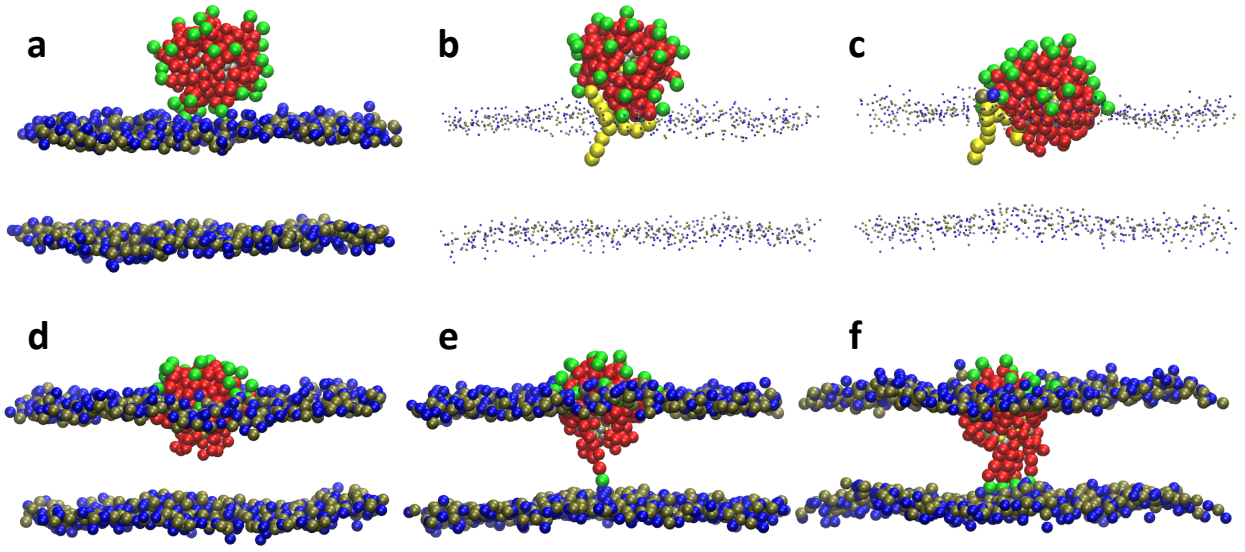

Figure 2. **a** stage 1, adsorption of the NP at the membrane surface; **b**-**d** stage 2, the protrusion of a lipid tail initiates the hydrophobic contact that leads to partial embedding of the NP in the membrane core; **e**-**f** the NP binds to the opposite leaflets (one and five anchors shown). The NP hydrophobic beads are shown in red, the charged NP beads in green. Lipid heads are blue (choline) and tan (phosphate), lipid tails are not shown, except for **b** and **c** where the protruding

lipid is shown with yellow tails. Water is not shown. All snapshots refer to a MUS:OT 1:1 random NP.

Stage 3: step-by-step to the snorkeling configuration. During the third interaction stage, the NP stabilizes its position within the membrane core by dropping one charged ligand to the head region of the opposite leaflet (Figure 2e). The first anchor is followed by a second, a third, and so on (Figure 2f, in our 20 μs runs the maximum number of anchors we observed is 6), leading to the snorkeling configuration predicted by thermodynamic models[23] and observed in charged dendrimers[24].

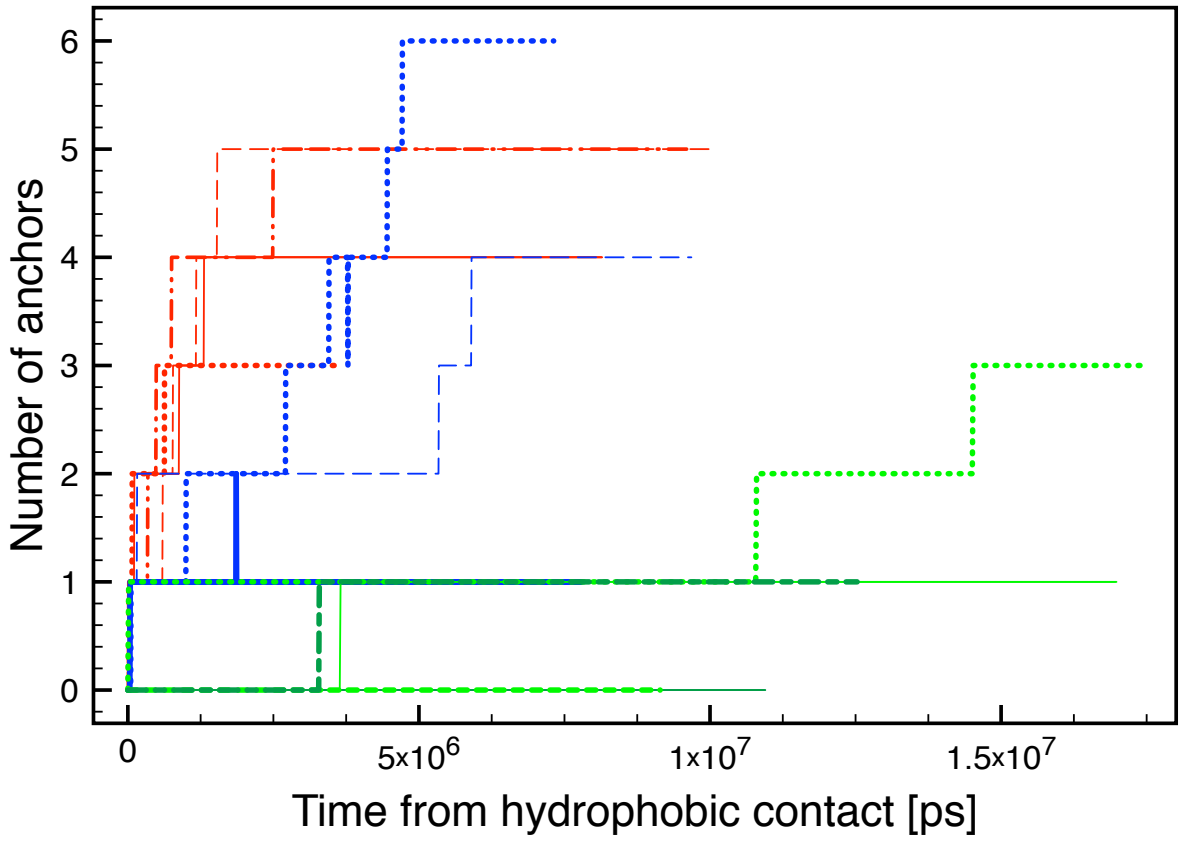

Figure 3. The number of anchors dropped by the NPs as a function of time, starting from the

creation of the hydrophobic NP-membrane contact. Different lines refer to independent simulations of random MUS:OT 1:1 (4 runs, red), random MUS:OT 2:1 (3 runs, blue) and patched MUS:OT 1:1 NPs (5 runs, green).

From kinetics to thermodynamics. The life times of the different stages of the interaction process span a broad time range, and depend on the type of NP. The average time spent by the NP in stage 1 is 6 μs, with no major differences observed for the NPs with different surface ligand arrangements (in two cases the NP remained in stage 1 for the whole run, and we did not include these in the average; see the Supplementary Table 1). Such a long time interval has hindered the observation of the spontaneous formation of the hydrophobic contact in previous atomistic[14,16] simulations, while CG simulations[17] focused on larger nanoparticles, whose kinetics of interaction is likely to be slower. The kinetics emerging from our simulations also suggests that the free energy landscape has a quite hidden saddle point that needs to be crossed to move to stage 2. In agreement with the hypothesis of Van Lehn *et al*.[15,16], our unbiased simulations show that the saddle point corresponds to the protrusion of a lipid tail, which energetic cost has been estimated in the 4-11 k_BT range[16].

In Figure 3 we plot the number of anchors dropped by the three different NPs we considered, as a function of the time elapsed since the formation of the hydrophobic contact. For random NPs, the time lag between the formation of the hydrophobic contact and the dropping of the first anchor is of the order of a few ns (see Figure 3). This suggests that a very small energy barrier needs to be overcome to lead random NPs from stage 2 to stage 3. Patched NPs, instead, can linger in stage 2 for much longer (5 ns, 3.7 μs, 3.9 μs, 9.3 μs and > 10.8 μs; indeed, the latter run ended before stage 3 was reached). This behavior indicates that, in the case of patched NPs, a

higher energy barrier hinders the transition to stage 3. We quantified via Metadynamics calculations (see the Supporting Information for the details) the energy barrier that one charged ligand of the patched NPs has to overcome to cross the hydrophobic core of the membrane and anchor to the opposite leaflet. The resulting free energy profile is shown in Figure 4. The charged ligand has to cross a barrier of about 9 k_BT to reach a saddle point, located 0.5 nm off the membrane centre. Then, it stably binds to the opposite leaflet – the recrossing implying the overcoming of a barrier that is twice as high. Indeed, we never observe anchor detachments in our simulations (Figure 3), either for the patched or random NP.

We performed Metadynamics calculations on the charged terminals of random NPs, as well. In this case, the sampling of the stage 2 → stage 3 transition is made difficult by the fact that, before the stage 2 → stage 3 crossing of the biased ligand has been sampled, other ligands spontaneously anchor to the opposite leaflet, making the free energy sampling of the first anchoring event impossible. The average life time of stage 2, in the case of random NPs, is three orders of magnitude shorter than for patched NPs. Such a difference would be compatible with a free energy barrier of a few k_BT, as sketched in Figure 4. We managed to sample by metadynamics, though, the recrossing process, concluding that the height of the recrossing barrier is similar in the random and patched cases (see Figure 4 and the Supporting Information for more details on the metadynamics calculations).

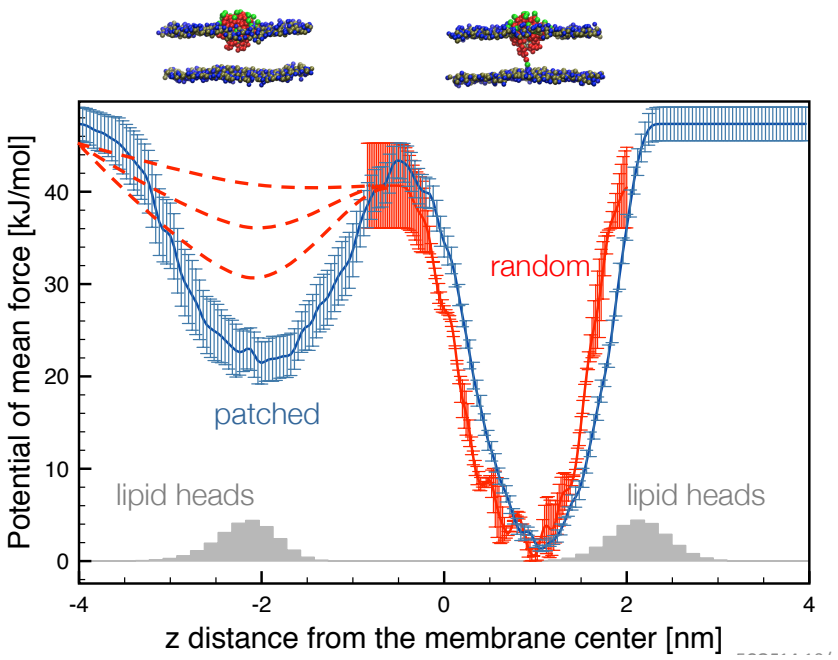

Figure 4. Free energy profiles related to the transfer of a negatively charged ligand terminal from the entrance leaflet to the opposite one. The blue and red profiles are related to the MUS:OT 1:1 patched and random ligand arrangement, respectively. Grey shades show the position of the polar lipid head beads (arbitrary units). Metadynamics data are shown with errorbars, while the red dashed lines are hypothesized profiles for the stage 2 → stage 3 transition of random NPs.

Our first conclusion, supported by the unbiased MD simulations and by our free energy calculations, is that monolayer-protected, partially anionic NPs penetrate in the membrane core of zwitterionic membranes. The energy cost associated to the extraction of a NP out of the membrane core is very high, making the anchoring process almost irreversible.

Furthermore, we have shown that the kinetics of the process is strongly influenced by the surface ligand arrangement. The free energy landscape of NPs with a random surface distribution of hydrophobic and anionic ligands is characterized by two metastable states, one corresponding to

the adsorption at the membrane surface, the other corresponding to the snorkeling configuration. NPs with a patched surface arrangement of anionic and hydrophobic ligands, instead, interact with the membrane moving through three metastable states. The third state is intermediate between the adsorbed and the snorkeling configuration, and corresponds to the formation of a stable hydrophobic contact between the NP and the membrane. The life time of this intermediate state is of the order of several microseconds. In a realistically crowded membrane environment, the different kinetics of the interaction of random and patched NPs might drive to different interactions of the NPs with other membrane constituents or membrane-embedded proteins, eventually leading to different translocation pathways.

ASSOCIATED CONTENT

Supporting Information. The Au NP and ligand model; the set-up and parameters of the MD simulations; the parameters used in the metadynamics calculations; the model validation; a list of all the simulations performed and the complete analysis of the MD simulations. This material is available free of charge via the Internet at http://pubs.acs.org."

AUTHOR INFORMATION

Corresponding Author

*Email: rossig@fisica.unige.it

Notes

The authors declare no competing financial interests.

ACKNOWLEDGMENT

Giulia Rossi acknowledges funding from the FP7 Marie Curie Career Integration Grant PCIG13-GA-2013-618560. Most of the simulations were performed at CINECA under the NANOPLAS (HP10CM4EYY) and BioGOLD (HP10CIBH54) grants.

REFERENCES

(1) Kennedy, L. C.; Bickford, L. R.; Lewinski, N. a; Coughlin, A. J.; Hu, Y.; Day, E. S.; West, J. L.; Drezek, R. a. A New Era for Cancer Treatment: Gold-Nanoparticle-Mediated Thermal Therapies. *Small* **2011**, *7*, 169–183.

(2) Dreaden, E. C.; Mackey, M. a; Huang, X.; Kang, B.; El-Sayed, M. a. Beating Cancer in Multiple Ways Using Nanogold. *Chem. Soc. Rev.* **2011**, *40*, 3391–3404.

(3) Dreaden, E. C.; Alkilany, A. M.; Huang, X.; Murphy, C. J.; El-Sayed, M. a. The Golden Age: Gold Nanoparticles for Biomedicine. *Chem. Soc. Rev.* **2012**, *41*, 2740–2779.

(4) Gao, J.; Gu, H.; Xu, B. Multifunctional Magnetic Nanoparticles: Design, Synthesis, and Biomedical Applications. *Acc. Chem. Res.* **2009**, *42*, 1097–1107.

(5) Häkkinen, H. The Gold-Sulfur Interface at the Nanoscale. *Nat. Chem.* **2012**, *4*, 443–455.

(6) Leroueil, P. R.; Berry, S. a; Duthie, K.; Han, G.; Rotello, V. M.; McNerny, D. Q.; Baker, J. R.; Orr, B. G.; Holl, M. M. B. Wide Varieties of Cationic Nanoparticles Induce Defects in Supported Lipid Bilayers. *Nano Lett.* **2008**, *8*, 420–424.

(7) Goodman, C. M.; McCusker, C. D.; Yilmaz, T.; Rotello, V. M. Toxicity of Gold Nanoparticles Functionalzied with Cationic and Anionic Side Chians. *Bioconju. Chem.* **2004**, *15*, 897–900.

(8) Tatur, S.; Maccarini, M.; Barker, R.; Nelson, A.; Fragneto, G. Effect of Functionalized Gold Nanoparticles on Floating Lipid Bilayers. *Langmuir* **2013**, *29*, 6606–6614.

(9) Van Lehn, R. C.; Atukorale, P. U.; Carney, R. P.; Yang, Y.-S.; Stellacci, F.; Irvine, D. J.; Alexander-Katz, A. Effect of Particle Diameter and Surface Composition on the Spontaneous Fusion of Monolayer-Protected Gold Nanoparticles with Lipid Bilayers. *Nano Lett.* **2013**, *13*, 4060–4067.

(10) Xi, A.; Bothun, G. D. Centrifugation-Based Assay for Examining Nanoparticle-Lipid Membrane Binding and Disruption. *Analyst* **2014**, *139*, 973–981.

(11) Sabella, S.; Carney, R. P.; Brunetti, V.; Malvindi, M. A.; Al-Juffali, N.; Vecchio, G.; Janes, S. M.; Bakr, O. M.; Cingolani, R.; Stellacci, F.; et al. A General Mechanism for Intracellular Toxicity of Metal-Containing Nanoparticles. *Nanoscale* **2014**, *6*, 7052–7061.

(12) Carney, R. P.; Carney, T. M.; Mueller, M.; Stellacci, F. Dynamic Cellular Uptake of Mixed-Monolayer Protected Nanoparticles. *Biointerphases* **2012**, *7*, 17.

(13) Verma, A.; Uzun, O.; Hu, Y.; Hu, Y.; Han, H.-S.; Watson, N.; Chen, S.; Irvine, D. J.; Stellacci, F. Surface-Structure-Regulated Cell-Membrane Penetration by Monolayer-Protected Nanoparticles. *Nat. Mater.* **2008**, *7*, 588–595.

(14) Heikkilä, E.; Martinez-Seara, H.; Gurtovenko, A. a; Vattulainen, I.; Akola, J. Atomistic Simulations of Anionic Au144(SR)60 Nanoparticles Interacting with Asymmetric Model Lipid Membranes. *Biochim. Biophys. Acta* **2014**, *1838*, 2852–2860.

(15) Van Lehn, R. C.; Ricci, M.; Silva, P. H. J.; Andreozzi, P.; Reguera, J.; Voïtchovsky, K.; Stellacci, F.; Alexander-Katz, A. Lipid Tail Protrusions Mediate the Insertion of Nanoparticles into Model Cell Membranes. *Nat. Commun.* **2014**, *5*, 4482.

(16) Van Lehn, R. C.; Alexander-Katz, A. Pathway for Insertion of Amphiphilic Nanoparticles into Defect-Free Lipid Bilayers from Atomistic Molecular Dynamics Simulations. *Soft Matter* **2015**, *11*, 3165–3175.

(17) Gkeka, P.; Angelikopoulos, P.; Sarkisov, L.; Cournia, Z. Membrane Partitioning of Anionic, Ligand-Coated Nanoparticles Is Accompanied by Ligand Snorkeling, Local Disordering, and Cholesterol Depletion. *PLoS Comput. Biol.* **2014**, *10*, e1003917.

(18) Van Lehn, R. C.; Alexander-Katz, A. Free Energy Change for Insertion of Charged, Monolayer-Protected Nanoparticles into Lipid Bilayers. *Soft Matter* **2014**, *10*, 648.

(19) Gkeka, P.; Sarkisov, L.; Angelikopoulos, P. Homogeneous Hydrophobic–Hydrophilic Surface Patterns Enhance Permeation of Nanoparticles through Lipid Membranes. *J. Phys. Chem. Lett.* **2013**, *4*, 1907–1912.

(20) Marrink, S. J.; Risselada, H. J.; Yefimov, S.; Tieleman, D. P.; de Vries, A. H. The MARTINI Force Field: Coarse Grained Model for Biomolecular Simulations. *J. Phys. Chem. B* **2007**, *111*, 7812–7824.

(21) Lee, H.; Larson, R. G. Molecular Dynamics Simulations of PAMAM Dendrimer-Induced Pore Formation in DPPC Bilayers with a Coarse-Grained Model. *J. Phys. Chem. B* **2006**, *110*, 18204–18211.

(22) Heikkilä, E.; Gurtovenko, A. A.; Martinez-seara, H.; Häkkinen, H.; Vattulainen, I.; Akola, J. Atomistic Simulations of Functional Au 144 (SR) 60 Gold Nanoparticles in Aqueous Environment. *J. Phys. Chem. C* **2012**, *116*, 9805–9815.

(23) Van Lehn, R. C.; Alexander-Katz, A. Fusion of Ligand-Coated Nanoparticles with Lipid Bilayers: Effect of Ligand Flexibility. *J. Phys. Chem. A* **2014**.

(24) Lee, H.; Larson, R. G. Membrane Pore Formation Induced by Acetylated and Polyethylene Glycol-Conjugated Polyamidoamine Dendrimers. *J. Phys. Chem. C* **2011**, *115*, 5316–5322.